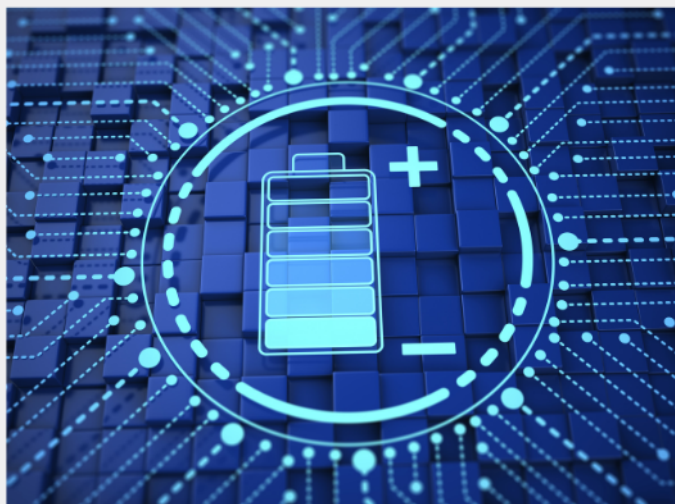




Exploring the possibilities of increasing energy density and efficiency in rechargeable batteries

Download this complimentary article collection



The exponential rise in the need for better, more efficient power sources has sparked an incredible amount of research into batteries. A primary focus of research has been increasing the energy density of batteries, as it allows for lighter, more portable storage of energy. Lithium-ion batteries, for example, have a much higher energy density than conventional lead-acid batteries and can be used for various purposes, such as in electric vehicles.

This article collection provides a comprehensive list of references for new methods and technologies for increasing the energy density of batteries.



WILEY

Unexpected Quasi-Axial Conformer in Thermally Activated Delayed Fluorescence DMAC-TRZ, Pushing Green OLEDs to Blue

Kleitos Stavrou,* Larissa G. Franca, Tobias Böhmer, Luka M. Duben, Christel M. Marian,* and Andrew P. Monkman*

Hidden photophysics is elucidated in the very well-known thermally activated delayed fluorescence (TADF) emitter, DMAC-TRZ. A molecule that, based on its structure, is considered not to have more than one structural conformation. However, based on experimental and computational studies, two conformers, a quasi-axial (QA) and a quasi-equatorial (QE) are found, and the effect of their co-existence on both optical and electrical excitation is explored. The relative small population of the QA conformer has a disproportionate effect because of its strong local excited state character. The energy transfer efficiency from the QA to the QE conformer is high, even at low concentrations, dependent on the host environment. The current accepted triplet energy of DMAC-TRZ is shown to originate from the QA conformer, completely changing the understanding of DMAC-TRZ. The contribution of the QA conformer in devices helps to explain the good performance of the material in non-doped organic light-emitting diodes (OLEDs). Moreover, hyperfluorescence (HF) devices, using v-DABNA emitter show direct energy transfer from the QA conformer to v-DABNA, explaining the relatively improved Förster resonance energy transfer efficiency compared to similar HF systems. Highly efficient OLEDs where green light (TADF-only devices) is converted to blue light (HF devices) with the maximum external quantum efficiency remaining close to 30% are demonstrated.

characteristic of efficient OLEDs is the exciton harvesting in the active layer of a device, which due to spin statistics forms 25% singlet and 75% triplet states.^[1–3] The triplet state utilisation is forbidden by Pauli's principle and internal quantum efficiency (IQE) is limited to 25% for fluorescence materials.^[4,5] Two classes of organic materials, the phosphorescent and the thermally activated delayed fluorescence (TADF) materials can overcome this problem by harvesting the triplet states.^[6,7] Phosphorescent materials containing heavy atoms enhance the strong spin-orbit coupling (SOC) and activate triplet state radiative decay.^[8] TADF molecules can convert triplet states into an emissive singlet state by reverse intersystem crossing (rISC) between the two states. This process is identified to be thermally activated by the vibrationally coupled spin-orbit coupling mechanism, which is facilitated by a small energy gap between the triplet and singlet state (ΔE_{ST}) and the use of a third state to

mediate the exchange.^[9–12]

Conventional TADF molecules contain a donor (D) and an acceptor (A), a structure that promotes the formation of an intramolecular charge transfer (ICT) state between the two moieties.^[13] This type of D-A molecule is characterized by an effective separation of the highest occupied molecular orbital (HOMO) and lowest unoccupied molecular orbital (LUMO) in the excited state through a near-orthogonal D-A relative orientation. The latter, minimizes the electron exchange energy to achieve very small ΔE_{ST} (typically below 200 meV) and enables efficient rISC at room temperature.^[14–16] The presence of a ³LE state (locally excited) within the ΔE_{ST} energy range, to vibrationally mix with the ³CT (charge transfer), enhances rISC by allowing SOC with the ¹CT.^[7,17–20]

In these already complex systems, extra parameters such as: intermolecular interactions between the same type of molecules (dimer/excimer) and different types of molecules (complex/excimer), guest-host interactions (environmental dipole moment effect)^[21] and conformational effects complicate the systems even more. On the latter, two types of conformation effects have been mainly explored so far: the distribution of

1. Introduction

Organic Light Emitting Diodes (OLEDs) are a valuable alternative to conventional light-emitting devices. A key

K. Stavrou, L. G. Franca, A. P. Monkman
Department of Physics
Durham University
Durham DH1 3LE, UK
E-mail: kleitos.stavrou@durham.ac.uk; a.p.monkman@durham.ac.uk
T. Böhmer, L. M. Duben, C. M. Marian
Institute of Theoretical and Computational Chemistry
Heinrich-Heine-University Düsseldorf
40204 Düsseldorf, Germany
E-mail: Christel.Marian@hhu.de

 The ORCID identification number(s) for the author(s) of this article can be found under <https://doi.org/10.1002/adfm.202300910>.

© 2023 The Authors. Advanced Functional Materials published by Wiley-VCH GmbH. This is an open access article under the terms of the Creative Commons Attribution License, which permits use, distribution and reproduction in any medium, provided the original work is properly cited.

DOI: 10.1002/adfm.202300910

dihedral angles between the D-A moieties^[22–24] and the possible ground and/or excited state conformers (i.e., planar, axial, equatorial etc).^[25–27] In the context of the second type of conformational effect, several D-A and D-A-D molecules have been reported whose donor unit is non-planar, leading to two configurations where the D-A are near orthogonal, i.e., axial and equatorial orientations.^[26]

In 2014, Tanaka et al. reported PTZ-TRZ, a structural analogue of PXZ-TRZ that has a sulfur atom instead of oxygen in the donor unit.^[25] This distorted the donor allowing axial and equatorial conformations to co-exist, and dual emission was observed originating from two ICT transitions derived from conformational heterogeneity (quasi-axial (QA) and quasi-equatorial (QE)). A similar effect was shown by Su et al., but instead of using a hetero atom, adamantane was attached to the acridine donor, showing the same dual conformational emission.^[28] Other cases of D-A systems also presented dual conformer emission.^[29] Such conformers in D-A-D systems have also been reported, and their photophysical behavior has been described in detail.^[26,30]

In this work, we investigate the TADF emitter DMAC-TRZ,^[31] a molecule that does not fulfill the requirements presented before to have dual conformer emission. Surprisingly, under specific conditions a QA conformer can be observed, although the QE conformer appears to be dominant. In solution state, the molecular interconversion from the QA to the QE is labile and the emission from the first only contributes to a very small extent. In solid-state however, because of the environmental restrictions (hindering molecular relaxation) the QA emission appears stronger. At low temperatures this effect is even stronger, while a structured QE CT emission can also be observed. The energy transfer process between the two conformer species appears to be very efficient, even at concentrations below 0.1 wt.%, and the TADF efficiency appears to increase with increasing concentration. Above 1 wt.% concentration, aggregation occurs and it appears to dominate above 5 wt.% loading, however, this enhances the TADF efficiency. Under specific conditions, at low temperature, the origin of the phosphorescence spectrum appears to come from the QA conformer, mainly because the lowest lying triplet state of the QE conformer has a pure CT character and if it can decay radiatively any phosphorescence would be vanishingly weak. In OLEDs the QA conformer appears to efficiently transfer its energy to the QE conformer and only in specific hosts a QA contribution can be seen. Using DMAC-TRZ as a sensitizer in hyperfluorescence (HF) OLEDs^[32–34] the QA conformer can directly pump the terminal emitter (because of the terminal emitter higher oscillator strength and better spectral overlap compared to DMAC-TRZ QE conformer). Thus, Förster resonance energy transfer (FRET) from the QA conformer to the terminal emitter outcompetes the FRET from the QA to the QE conformer. This significantly improves the FRET efficiency of the system, compared to similar sensitizer-terminal emitter systems. HF OLEDs with maximum external quantum efficiency (EQE_{max}) close to 30% were fabricated but most importantly, a green TADF sensitizer was converted to blue HF OLED for the first time.

2. Results and Discussion

2.1. Basic Photophysics

The solvatochromic behavior of DMAC-TRZ in both excitation and emission measurements is shown in **Figure 1**. In MCH the excitation spectrum has two distinct bands with peaks at 376 nm (Ab1) and 413 nm (Ab2). Upon increased solvent polarity, the Ab2 band decreases in intensity and a tail appears at 450 nm, an expected behavior for a CT excited state, but loses in oscillator strength with increasing polarity. The Ab1 band appears unaffected and slightly blue-shifted in acetonitrile (CH_3CN).

Deconvolution of the excitation spectra in the four different solvents, using two Gaussians, shows an Ab1 band maximum of ≈ 376 nm in all cases (with a minor 5 nm hypsochromic shift in CH_3CN), and a full width half maximum (FWHM) of 55 ± 4 nm (Figure S1, Supporting Information). This behavior is expected from a strongly localized excited state. The Ab2 band maximum is observed at 413 nm in all solvents but reduces in intensity and increases in FWHM (from 35 nm in MCH to 63 nm in CH_3CN) with increasing solvent polarity. The latter follows the FWHM behavior of the emission spectrum (Figure 1b) and is undoubtedly from the CT state between the donor and acceptor moiety. The Ab2 band appears to have a mixed, local (LE) and CT character in MCH, giving a structured excitation and photoluminescence (PL) spectrum.

In MCH and upon excitation at wavelengths between 320 and 380 nm, a shorter wavelength emission band appears (Em1) with an emission maximum at 390 nm (Figure S2b, Supporting Information). The relative intensity of the Em1 band maximum is the highest when exciting at 360 nm, where the intensity of the Ab1 band is close to its maximum, and the Ab2 band is close to its minimum value (Figure S1a, Supporting Information). Interestingly, when exciting at shorter wavelengths ($\lambda_{\text{exc}} < 310$ nm) the Em1 band is not observed. The excitation profile of the Em1 band is well resolved, solvent independent (Figure S3a, Supporting Information) and appears very similar to the deconvoluted Ab1 spectra (Figures S1a and S2a, Supporting Information). With increasing solvent polarity, the relative PL intensity of Em1 band decreases and its peak position has a minor redshift, compared to the main PL (Em2) band (Figure 1b; Figure S3b, Supporting Information). The absorption and emission spectra of the individual D and A units were studied previously and are energetically in higher positions compared to the Ab1 and Em1, respectively.^[35] Hence, these two distinct emission bands (Em1 and Em2) can only be assigned to two different conformers of the DMAC-TRZ molecule.^[26]

Similar behavior is observed using a zeonex polymer matrix as a host (Figure S4, Supporting Information). Due to the steric hindrance from the solid-state matrix, conformational relaxation (or interconversion) is prevented to a much higher degree, in contrast to the solvent environments. Consequently, the Em1 band is more intense and provides better resolved excitation spectra upon collections between 390–420 nm (Figure S4a, Supporting Information). From the excitation spectra, two isosbestic points are observed, one at 325 nm and another at 390 nm, which suggest the presence of two distinct species.

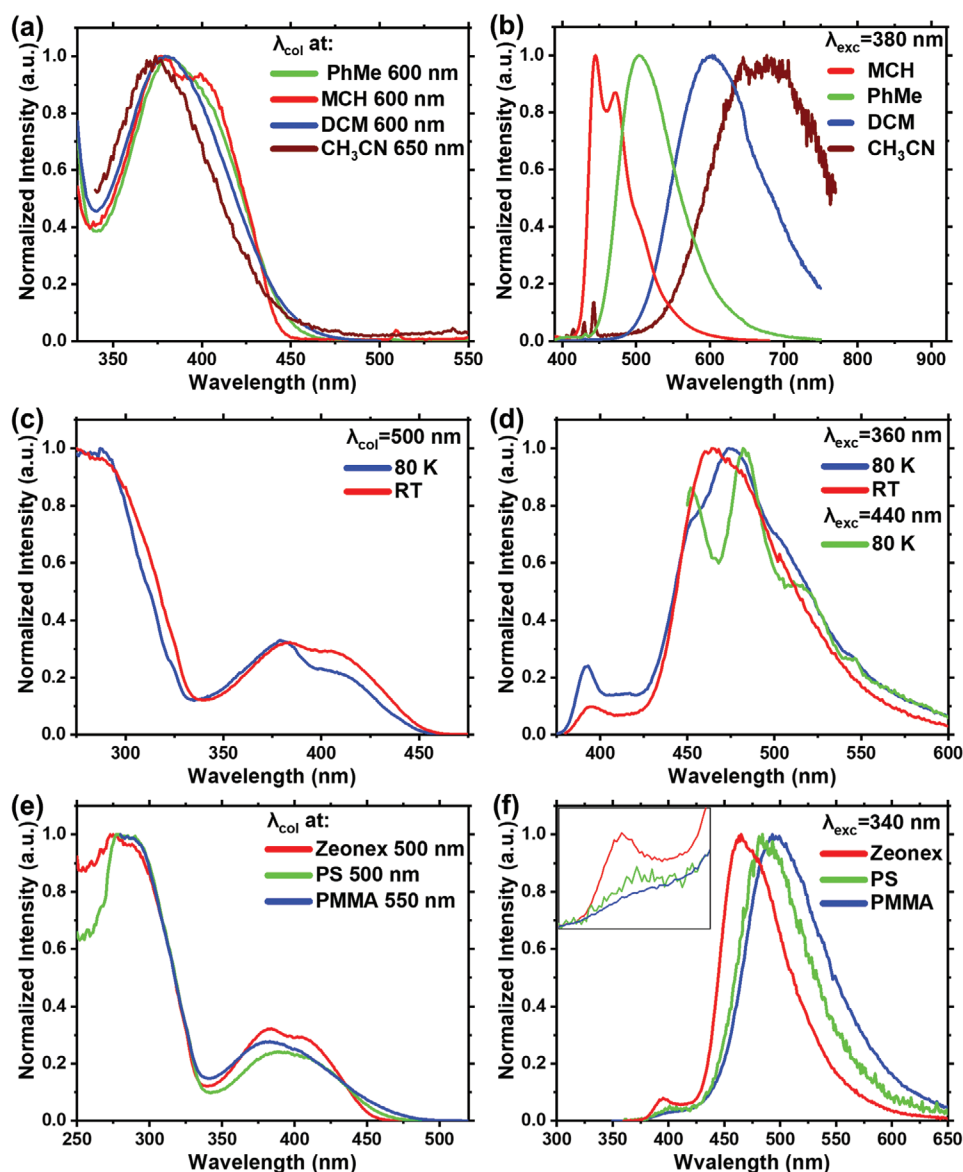


Figure 1. Steady state photophysics of DMAC-TRZ. a) Excitation and b) PL spectra of 20 μM concentration of DMAC-TRZ in different solvents, at room temperature. c) Excitation and d) PL spectra of 1 wt.% DMAC-TRZ in zeonex host, at room temperature (red) and 80 K (blue). e) Excitation and f) PL spectra of 1 wt.% DMAC-TRZ in different polymer hosts, at room temperature. Inset: Zoom in on the high energy band.

It is important to reiterate that the contribution of the local D and A units (below 325 nm) to the excitation spectra is minimal when collecting at wavelength where only Em1 emits. Low temperature steady state measurements of the same film show that the increased hindrance introduced by freezing the environment enhances the relative contribution of the Em1 band (Figure 1d; Figure S5, Supporting Information). From excitation spectra, a decrease in relative intensity of the Ab2 band and a better resolved Ab1 band can be observed (Figure 1c), while the Stokes shift between Ab1 and Em1 is very small (Figure S5d, Supporting Information). The Em2 band is more structured when compared to room temperature and appears better resolved upon direct excitation of the Ab2 band only (Figure 1d, green curve). This indicates that excess excitation energy broadens the spectrum. Here it is important to mention

that the phosphorescence contribution to the total DMAC-TRZ emission, even at low temperature, is minimal as shown in our previous studies.^[23]

Using two polymer hosts with stronger ground state dipole moment (*i.e.*, enhanced relative polarity) a bathochromic shift is observed in the Em2 band, both in excitation and emission spectra (Figure 1e,f). In polystyrene (PS), the Em1 band appears reduced in intensity by a factor of two (Figure S6, Supporting Information), while in PMMA by a factor of three (Figure S7, Supporting Information) compared to zeonex. The onset of the Em1 band appears to be the same in all cases while the peak has a small bathochromic shift and appears less resolved. This indicates that the excited state of Em1 conformer has a mixed (LE & CT) but stronger LE character compared to the Em2 CT conformer state (Figure 1f). Again, upon excitation at wavelengths

below 310 nm the Em1 is not observed. By collecting at the Em1 emission band, the excitation spectra are identical in all hosts (Figure S8, Supporting Information). The latter is in good agreement with the solution results, see above.

Small molecule hosts were also used, and the two bands were again observed in various hosts (Figure S9, Supporting Information). Unfortunately, the most common carbazole based hosts often used in OLED devices could not be used as most of them emit in the same region as the higher energy conformer (Em1), such as the case of BCPO. The UGH spectrum looks similar to the one in zeonex, with a small increase in the relative intensity due to possible extra steric hindrance from the host. DPEPO has a much smaller contribution from the Em1 band due to the shift of the CT absorption resulting to a better energy transfer from the high energy conformer (Em1) to the low one (Em2). Finally, neat film does not have any contribution from the Em1 band mainly because the intermolecular distance is minimal increasing the FRET efficiency between the two conformers.

2.2. Calculations

Quantum chemical calculations are used to understand the nature of these conformers. Two stable conformers of DMAC-TRZ, a QE conformer with planar DMAC donor and TRZ acceptor moieties arranged perpendicular to one another (Figure 2c) and a QA conformer in which DMAC adopts a kinked structure tilted by $\approx 40^\circ$ with respect to the TRZ plane (Figure 2d). In MCH solution, the QE conformer is favored over the QA conformer by 0.19 eV including zero-point vibrational energy (ZPVE) corrections and hence represents the

majority component. Combined density functional theory and multi-reference configuration interaction (DFT/MRCI) calculations yield vertical excitation energies of 3.06 eV (405 nm, Ab2) and 3.35 eV (371 nm, Ab1) for the S_1 states of the QE and QA conformers, respectively which compare favorably with the experimentally observed band maxima in this solvent (Figure 1b). However, while the $S_1 \leftarrow S_0$ transition of the QA minority conformer is characterized by a mixed CT/LE excitation with high oscillator strength, the $S_1 \leftarrow S_0$ CT transition of the C_{2v} -symmetric QE conformer is electric dipole forbidden in Franck–Condon (FC) approximation. Coupling between the electronic degrees of freedom and torsional vibrations about the molecular axis lends intensity to this CT transition which therefore becomes weakly allowed in Herzberg–Teller (HT) approximation (Figure S10) and for ensemble averages. That both peaks are observed with nearly equal intensity in the excitation spectrum is thus a consequence of the small concentration of the optically very bright QA conformer in MCH solution on the one hand and the necessity to vibronically enhance the electric dipole-forbidden transition of the QE majority conformer on the other hand. Examination of the experimentally measured QE absorption band (Ab2) in MCH reveals a weak vibrational structure arising from the vibronic coupling to the electronic transition (Figure 2a). The estimated vibronic energy spacing of this HT transition is 1170 cm^{-1} indicative of a coupled C–N band stretch,^[36] most likely the C–N bridging bond between D and A. Even small changes in this bond length and torsion will radically change the radiative coupling, highlighting the sensitivity and important role of the C–N donor acceptor bridging bond plays in these TADF materials.

With regard to the photophysics of the QE conformer, the presence of a $T_{LE(TRZ)}$ state in energetic proximity of the

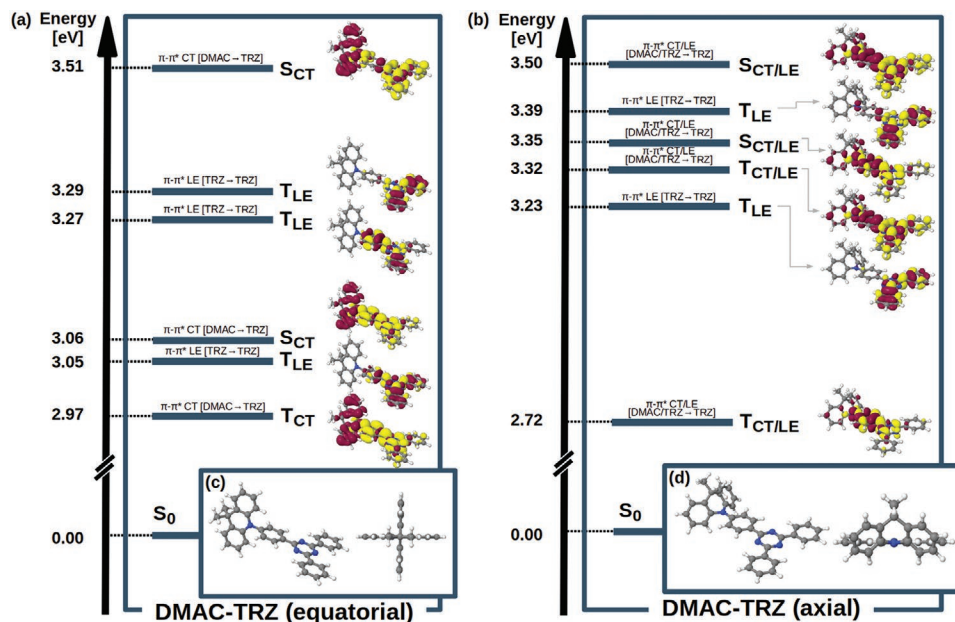


Figure 2. Calculated vertical DFT/MRCI excitation energies and state characteristics of the a) QE and b) QA conformers of DMAC-TRZ at the respective ground-state geometry in methylcyclohexane solution. The QE conformer is favored over the QA conformer by 0.19 eV including ZPVE corrections. A loss of electron density w.r.t. the electronic ground state is indicated in red, a gain in yellow. Geometric structures of the c) quasi-equatorial and d) quasi-axial conformers of DMAC-TRZ in the electronic ground state.

lowest-lying S_{CT} and T_{CT} states is noteworthy as it can mediate their ISC and rISC processes and lead to efficient TADF (Figure 2a).^[11,37] For the QA conformer, two triplet states are found to lie below the S_1 state and a third one lies slightly above the S_1 state in the FC region (Figure 2b). The substantial energy gap between the S_1 and T_1 states, caused by the local $\pi\pi^*$ contributions to their wavefunctions, rule out TADF for this conformer. A detailed computational study investigating the role of the higher-lying triplet states in the photophysical deactivation pathways of both conformers is currently under way and will be presented in the near future.

The oscillator strength (f) of the two conformers in MCH was calculated to be 0.00006 for the QE conformer and 1.09379 for the QA conformer. The big difference can be explained by the strong local character of the QA conformer, compared to the CT character of the QE conformer. The population of both conformers in MCH can be approximately estimated from the ratio of the absorbance to the oscillator strength for the two individual conformers. This results to an approximate ratio of 99.9:0.1 population of QE to QA conformers, in MCH solution. This estimated population is completely dependent on the theoretically estimated transition oscillator strengths. Rama et al., previously reported the phosphorescence and excitation spectrum of DMAC-TRZ in frozen solution.^[35] From the excitation spectrum results, which we now understand to include both QA and QE contributions, the QA population appears to be much larger in frozen solution at long delay times, compared to our estimate from room temperature MCH solution. This makes sense as the energy barrier crossing in solid state, which requires cooperative motion of the molecule, must be hindered, slowing down the interconversion and potentially giving a higher QA population. In solid state, and more specifically in evaporated films, where the solvent is not present, and the conformation entropy of the system will be different, the population of the QA conformer is expected to be much higher. Further, the QA conformer contribution in the PL spectrum is expected to be much higher due to matrix hindering possible interconversion between the two conformers, something that is possible in solution environments, especially with the presence of excess energy in the system. The latter is verified by the absence of the QA emission, in MCH solution, when exciting at wavelengths below 300 nm (Figure S2, Supporting Information).

2.3. Conformer Photophysics

At very low emitter concentrations (0.01 wt.%) in zeonex the maximum PL intensity of the QA conformer band (Em1) is comparable with that of the QE band (Em2) (Figure S11, Supporting Information). This observation can clearly be reconciled with low FRET due to the higher spatial separation between the individual molecules. With increasing concentration, the QA PL band decreases considerably in relative intensity monotonically (Figure S12, Supporting Information). Also, the high ground state dipole moment of DMAC-TRZ molecules, compared to the host, changes the ground state of the environment at higher concentrations (intermolecular interactions) and the QE absorption/emission stabilizes to a lower energy. Further, at

higher concentrations there will be a higher probability for excitons to reach lower energy states on average because exciton hopping is more efficient, leading to higher QE PL peak shift.

From Figure S11a (Supporting Information) spectra, the mixed CT/LE character of both bands is clear, especially in zeonex host, because of their structured PL emission. With increasing host dipole moment, both bands lose their structured shape, and shift towards longer wavelengths. The QA band has a small bathochromic shift of 115 meV, going from 395 nm in zeonex to 410 nm in PMMA, which could occur due to increasing overlap with the QE absorption band. The QE band shifts by 247 meV, going from 448 nm in zeonex to 490 nm in PMMA (Figure S11b, Supporting Information). This indicates that the QA and QE conformers have stronger LE and CT character, respectively.

Temperature dependent steady state spectra of 0.01 wt.% DMAC-TRZ in zeonex are shown in Figure S13 (Supporting Information). Upon exciting both conformers (at 360 nm), structured emission is observed from both at room temperature. By lowering the temperature, the QA emission (395 nm) increases in relative intensity indicating that a possible conformational interconversion of the QA to the QE conformation is hindered because of the frozen matrix and low temperature (it is not due to singlet exciton migration enhancing the FRET radius, as this is highly unlikely at 0.01 wt.% in zeonex). The QE emission is also affected by the temperature, becoming more structured and the spectral band maxima changing from the 0–0 transition to the 0–1 transition. This effect is also observed with direct excitation ($\lambda_{exc} > 400$ nm) of the QE CT (Figure S13, Supporting Information) and is attributed to hindering of the torsion motions because of the frozen environment, and the spectra are better resolved. Further, in all PL spectra there is a weak emission band ≈ 500 nm which increases in relative intensity with decreasing temperature. This excited state can be directly populated upon excitation above 460 nm. To understand the origin of this band, excitation spectra at different collection wavelengths are shown in Figure S13b (Supporting Information). When collecting below 500 nm the behavior is the same as 1 wt.% in zeonex (Figure S5a, Supporting Information). Collecting above 500 nm, a further weak excitation band is observed between 450–500 nm (Figure S13b, Supporting Information). This new band does not appear in solution or at higher concentration solid state measurements and has the same structure at all temperatures. Thus, we can only assume that it is a dimer emission that can be formed in solid state, even at very low concentrations, and is only observed in low ground state dipole moment environments. It cannot be observed at higher concentrations or higher dielectric media because it overlaps with the redshifted CT emission. Nevertheless, the contribution of this species at room temperature can be considered minimal.

Using the Jacobian spectral (wavelength to eV) conversion, the PL spectra of 0.01 wt.% DMAC-TRZ in zeonex at 80 K and different excitations, we again identify three distinct emission bands (Figure S14a, Supporting Information). At 360 nm excitation, three regions with constant vibronic intervals are found; at high energy the QA conformer appears to have at least three observable vibronic contributions of 152 meV between 3.15 and 2.84 eV. After a short gap of 75 meV, the QE conformer

emits between 2.77 and 2.29 eV, again with 152 meV vibronic spacing. The third region below 2.29 eV has narrower spacing of 130 meV. Upon direct excitation of the low energy species (480 nm), the aggregated band appears well resolved with 130 meV vibronic spacing, similar to the 360 nm excitation (Figure S14b, Supporting Information).

The steady state behavior of 0.01 wt.% DMAC-TRZ in different polymer hosts is shown in Figure S15 (Supporting Information). An energy relaxation effect is observed upon excitation at 380 nm, which becomes less pronounced at lower temperatures for both the QA and QE conformers (Figure S15a, Supporting Information). The vibronic structure of the QE emission appears to be less defined in polystyrene and even less in PMMA. Exciting at 430 nm (mainly the QE conformer), the energy relaxation effect is clearer at room temperature, compared to 380 nm excitation, and reduces at lower temperatures (Figure S15b, Supporting Information). The latter could indicate that at low temperature the possible side group motions of the polymer chain are reduced, reducing the slow reorganizational effects that can lead to the relaxation of the CT energy.^[22] At 0.01 wt.% loading, this cannot be an effect of energy migration to low energy sites in the density-of-states (DOS). Upon excitation at 460 nm, in polystyrene and PMMA we still observe the temperature dependent energy relaxation effect on the QE CT state, with polystyrene giving a structured emission compared to higher excitation energies (Figure S15c, Supporting Information). The very weak red aggregated/dimer emission band ($PL_{\max} = 525$ nm) observed in zeonex cannot be observed in the other two hosts due to overlap with the QE CT PL. This can also be observed in the excitation spectra (Figure S16, Supporting Information).

Time-resolved spectra from 0.01 wt.% DMAC-TRZ in zeonex, at various temperatures are shown in Figures S3 and S17 (Supporting Information). At early time (0.5 ns time delay) and all temperatures, the emission (395 nm) comes mainly

from the QA conformer (Figure S17a, Supporting Information), because of the faster radiative rate of the more strongly local character state. The contribution of the QE CT band is observed at 450 nm and appears to decrease in intensity with decreasing temperature, relative to the QA band. This verifies that the frozen matrix hinders the molecular relaxation of the QA to the QE conformation, resulting in a higher QA population, and thus stronger emission from the QA conformer at early times (<10 ns) (Figure 3a). At later prompt fluorescence (PF) times, the emission comes from the QE conformer and becomes more structured with decreasing temperature, indicating that under specific conditions a CT state can have vibronic character (note that the band does not blue shift at all).^[38] At μ s times, the room temperature measurement shows strong emission which comes from the QE CT band (Figure S17a, Supporting Information). In ms, the emission mainly comes from the phosphorescence with an energy onset of 2.75 eV (450 nm) and a small contribution of DF being observed at room temperature which decreases in contribution with decreasing temperature (small band below 450 nm). The PF emission area normalized spectra (Figure S17b, Supporting Information) clearly show the presence of two species (QA and QE conformer), with an iso-emissive point at 430 nm. A second iso-emissive point at 530 nm is only obvious at lower temperatures. This we assign to the aggregated species, as stated above.

The effect of temperature on the time-resolved spectra of 0.01 wt.% DMAC-TRZ in polystyrene and PMMA hosts are shown in Figure S18 (Supporting Information). In both cases a strong contribution from the QA conformer is observed in early times. Here it is worth mentioning that polystyrene and PMMA themselves emit at 380 nm, when excited at 355 nm (Figure S19, Supporting Information), but the PL contribution from the polystyrene is minor compared to the PMMA. As a result, the PMMA spectra have a strong contribution from the host itself (along with the QA emission) compared to the other

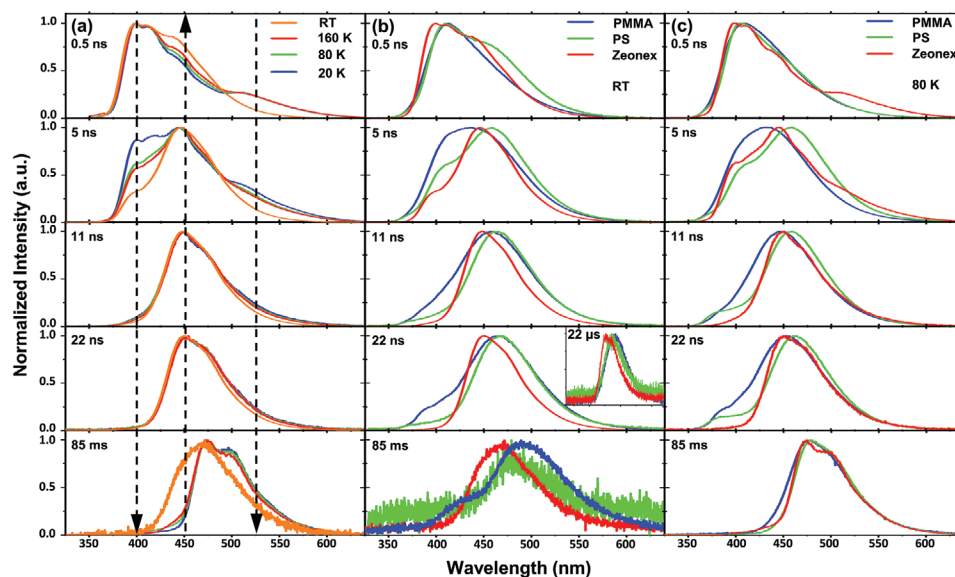


Figure 3. Time-resolved spectra of 0.01 wt.% DMAC-TRZ in a) zeonex at different temperatures and time delays. Time-resolved spectra of 0.01 wt.% DMAC-TRZ in three polymer hosts at different time delays at b) room temperature (Inset: DF spectra following the solvatochromism effect) and c) 80 K. Excitation wavelength 355 nm.

two hosts. At the later PF regime ($t > 10$ ns) both films have dual emission, the main band coming from the QE conformer and the high energy band (≈ 400 nm) from the host. In all three hosts, a high energy iso-emissive point is observed in the area normalized spectra, between QA and QE emission.

Comparing all three hosts one can see the large contribution from the QA conformer at early times, pumping the QE conformer which dominates after 10 ns and continues into the DF regime (Figure 3b). The QE TADF emission is clear at 22 μ s as shown in the inset of Figure 3b. At 85 ms delay time, DF can still be observed in all hosts with PMMA having a high energy band which appears similar to the PMMA phosphorescence emission. The phosphorescence spectra are similar in all cases, with an energy onset of 2.75 eV, being in good agreement with our previous results.^[23] PMMA film has slightly higher phosphorescence energy onset but is actually contribution for TADF emission, even at 80 K, because of the smaller ΔE_{ST} (Figure 3c).

Further analysis of the effect of the two conformers on the overall photophysics was made using time-resolved (TR) emission decays, shown in Figure 4. Zeonex host was chosen as a neutral environment. Upon excitation of the QA conformer at 375 nm, and collecting at 395 nm, where the QA conformer emits (Figure 4a), a dominant very fast component with lifetime less than 1.15 ns is found, contribution 86% (at 0.01 wt.%) and 99% (at 1 wt.%) (Figure 4b; Figure S20a, Supporting Information). This lifetime is assigned to the singlet lifetime of the QA conformer quenched by energy transfer to molecules in the QE conformation. This lifetime decreases with increasing concentration, as expected from a FRET related process.

The unquenched PF lifetime of (isolated) QA conformers is 71 ± 0.2 ns with a population that decreases with increasing concentration. A third component appears from 0.1 wt.% loading, having the same lifetime as the QE PF component (Figure S20a, Supporting Information). The latter indicates that even though the emission of the QE state at 395 nm should be minimal, as the FRET efficiency increases less unquenched QA emission occurs and QE emission can be observed.

Collecting at 550 nm, (375 nm excitation wavelength) mainly the QE conformer emission is monitored (Figure 4c). The lifetime behavior appears to be similar with increasing concentration, with only a minor increase from 13 ns (0.01 wt.%) to 16.9 ns (1 wt.%) as the concentration increases due to possible stronger contribution from intermolecular (dimer/excimer) states (Figure S20b, Supporting Information). Upon excitation at 405 nm, where the QE conformer mainly absorbs, the results appear to be similar with 375 nm excitation (Figure 4d).

A larger concentration series in zeonex, from 0.01 wt.% up to 25 wt.% DMAC-TRZ loading, was studied using time-resolved PL spectra, to highlight the effect of the QA conformer contribution (Figure S21, Supporting Information). At 0.01 and 1 wt.% concentration the QA contribution is dominant at early times. With increasing concentration, the intermolecular separation decreases and the FRET efficiency increases resulting in a better energy transfer from the QA to the QE conformer. Because of the latter, at 25 wt.% loading no QA contribution is observed. Increasing the emitter concentration also has an impact on the QE emission spectrum which appears to red-shift (Figure S21, Supporting Information). The emission

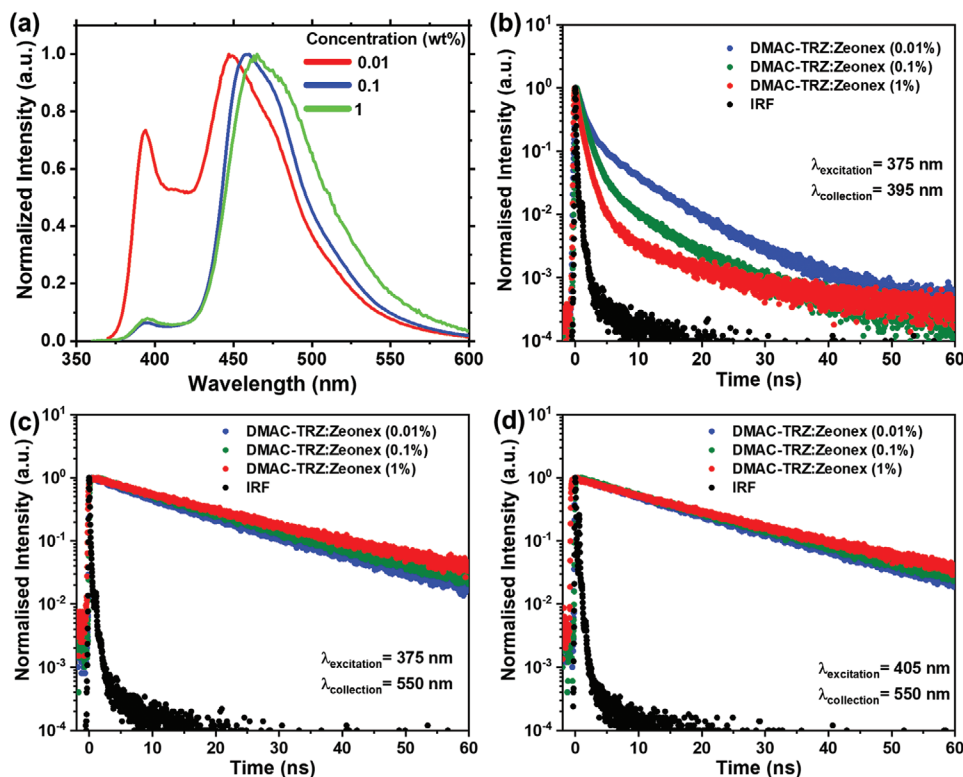


Figure 4. Photophysics of DMAC-TRZ in zeonex host, at different concentrations and room temperature. a) Steady state photoluminescence. b–d) time-resolved photoluminescence at different excitation and collection wavelengths.

spectrum of this band though appears to be the same in 5, 10, and 25 wt.%. The latter indicates that the ΔE_{ST} decreases with increasing concentration, up to a specific value (5 wt.%), due to the change of the environment's dielectric, and then remains stable.^[23] The small decrease in ΔE_{ST} appears to have a disproportionate effect on the increase in DF contribution, especially for concentrations above 1 wt.% (Figure S22, Supporting Information). This implies that other phenomena might have an impact on the DF contribution.

Any potential DF contribution from the QA conformer is not observed because the DF TR-PL spectra, at all concentrations, have the QE conformer profile. This is because FRET is orders of magnitude faster than ISC causing most excited states to be transferred to the QE ¹CT state even at very low concentrations. Instead, aggregate emission has already been observed in DMAC-TRZ guest-host systems, especially for concentrations above 10 wt.%.^[23] From the neat film PLQY, it is clear that the aggregated state (dimer/excimer) efficiency is high with a value of 75%, compared to nearly 100% at 10 wt.% doped film in mCBPCN host.^[23] Also, the through space analogue of DMAC-TRZ, TpAT-tFFO,^[39] that has among the best TADF performance, is basically an exciplex of controlled D-A distance. Thus, we believe that the enhanced DF contribution comes from a faster intermolecular k_{rISC} and not a change of the environment's dielectric (because of the increasing concentration of the dopant), at least not at concentrations above 5 wt.%. Nevertheless, despite the improved k_{rISC} , the aggregated emission state has lower PLQY than DMAC-TRZ monomer due to enhanced non-radiative pathways.

We have previously reported the DMAC-TRZ triplet value to be at 2.75 eV (450 nm).^[23] The triplet value of the individual donor and acceptor units have also been reported to have much higher values ($T_{D,A} > 3$ eV).^[35] In addition, TpAT-tFFO which is incapable of having a QA conformer, has been reported to have a ³CT character lowest triplet state,^[40] and its value depends on the distance between the D-A units. This experimentally has been difficult to prove and the lowest lying triplet energy was calculated to be above 3 eV.^[39] All the above imply that the 'low' triplet value observed in DMAC-TRZ could either be due to the state being of ³CT or of mixed ³(CT/LE) character. As a mixed ³(CT/LE) state is easier to observe, because the oscillator strength increases dramatically, we believe this is what we are observing in DMAC-TRZ and this then explains the structured phosphorescence emission observed in DMAC-TRZ, in specific environments (Figure S23, Supporting Information).

In our previous work^[23] we showed that the triplet energy of DMAC-TRZ is temperature dependent. At 20 K, the phosphorescence spectrum is blue shifted compared to that at 80 K, observed in all hosts and neat film, except zeonex where the phosphorescence spectrum is identical at both temperatures (Figure S23, Supporting Information). At 80 K in mCPCN and mCBPCN, where the triplet value of the host is only slightly higher than the triplet value of the DMAC-TRZ, a Gaussian shape emission spectrum appears with a wavelength onset of 460 ± 1 nm in both cases, which is redshifted compared to the DMAC-TRZ:zeonex film at the same temperature. Energetically it is at the same position as the low temperature DF (coming from the QE CT state), which appears to contribute in the delayed regime, even at low temperatures (as low as

80 K), because of the efficient k_{rISC} .^[23] At 20 K, in both hosts, where the DMAC-TRZ TADF contribution is minimal based on the time-resolved spectra,^[23] the phosphorescence spectrum is blue shifted and appears identical to the phosphorescence spectrum measured in films of neat hosts (Figure S23b,c, Supporting Information). The host phosphorescence is dominant at 20 K, because we excite both the host and the guest, so at very low temperatures some host triplet states do not migrate to the guest sites at 1 wt.% concentration, and can be observed because of their stronger oscillator strength compared to the DMAC-TRZ lowest lying triplet. This must then have a strong ³CT character. Although the host triplet appears to be the lowest observable triplet state of the system, this cannot be the case in the guest-host systems because DF emission from the QE ¹CT is observed at room temperature,^[23] which means that the up-converted QE ³CT are not quenched by the triplet of the host. Therefore, the lowest energy triplet of DMAC-TRZ QE conformer must be below that of these two hosts.

When the hosts lowest lying triplet energy is much higher compared to the guest, this effect does not occur. In DPEPO host ($T_1 \sim 3$ eV),^[41] the 80K phosphorescence spectrum of 1 wt.% DMAC-TRZ appears similar to that observed in mCBPCN and mCPCN hosts, another indication that DF is still observable at this temperature. At 20 K, a blue shift of the onset is observed towards 445 nm (from 460 nm), similar to the DMAC-TRZ:zeonex film, and far from the triplet value of DPEPO. In the absence of a host (i.e., neat film) a structured emission appears at 80 K with an onset of 475 nm, and is assigned to aggregated emission. Lowering to 20 K a second band appears, with the onset of the high energy band at 2.82 eV (440 nm), similar to what was observed in the high triplet energy hosts and in frozen solution^[35] (Figure S23e, Supporting Information). This indicates that the two conformers have distinct lowest triplet states. The QE conformer has a strong CT character triplet state, which must be energetically slightly below the ¹CT but is difficult to observe in all environments because of its low oscillator strength. This explains why in mCPCN and mCBPCN we see host phosphorescence but no guest phosphorescence. Thus, the triplet value observed at 20 K, in DPEPO and zeonex films is attributed to the QA triplet value (not the QE triplet), which has a mixed CT/LE character and so is emissive enough to be observed. This is in good agreement with the calculations (Figure 2).

Conformational heterogeneity^[23] is a parameter that could affect this determination, regarding the origin, of the triplet state discussed above. One could speculate that a molecule with lower dihedral twist angle between the donor and acceptor units could be the source of this triplet energy. Our previous studies,^[22-24] show that conformational heterogeneity is environment dependent. Thus, the population of the low twisted angle D-A molecules should decrease with increasing dielectric, and in high dielectric DPEPO host this population will be negligible, thus its phosphorescence would be difficult, if not impossible, to observe. Further, a QE ³CT with some local character should be easier to change with the environment dielectric, compared to a ³LE with some CT character (which is the case of the QA conformer). Thus, we verify that the lowest triplet observed in different environments, which is dielectric independent, could only be the triplet of the QA conformer.

2.4. Devices

Devices were fabricated with a structure of ITO (anode) | NPB (HTL, 40 nm) | TSBPA (EBL, 10 nm) | DMAC-TRZ x wt.% in different hosts (EML, 30 nm) | TPBi (HBL, 10 nm) | POT2T (ETL, 40 nm) | LiF (EIL, 1 nm) and Al (cathode, 100 nm). For the emissive layer (EML) a concentration series of 5, 15, and 25 wt.% DMAC-TRZ was used in a number of hosts with different ground state dipole moments (mCP, mCPCN, mCBPCN, BCPO, DPEPO, and neat film). The resultant EL spectra in each individual host are shown in Figure S24 (Supporting Information), and the contribution of the QA conformer appears in specific environments, similar to previous dual conformer emitter studies.^[25] The QA electroluminescence (EL) contribution is strongest in mCP and decreases in intensity with increasing host dielectric, because of better spectral overlap between the EL of the QA and the absorption of the QE conformer (which redshifts with increasing dielectric constant). In mCPCN, the QA contribution appears to be minor and seems to set the environment threshold for complete FRET between the two conformers. In BCPO and DPEPO no contribution from the QA conformer can be observed. Possible host emission is excluded because of their different emission spectra, as shown in Figure S24f (Supporting Information). Also, if the emission was coming from the hosts, it should have been observed in mCPCN and BCPO devices too. In all cases, where the QA emission is observed, its relative intensity appears to decrease with increasing DMAC-TRZ concentration, mainly because of increasing quenching by the QE conformers.

To investigate further the QA effect on OLEDs, a new set of devices using DMAC-TRZ as a triplet harvesting/singlet sensitizer for v-DABNA as a terminal emitter was fabricated in mCBPCN host (device structure in Figure 5). Using this approach one can investigate the effect of energy transfer to the v-DABNA from the two conformers. Figure S25a (Supporting Information) shows the absorption and emission overlap between v-DABNA and DMAC-TRZ respectively, a critical parameter for efficient FRET.^[32,42] To our understanding this system has the smallest spectral overlap so far reported yet achieves very high FRET efficiency, even at 1 wt.% v-DABNA loading.

The electrical response of the DMAC-TRZ only and HF-OLEDs appears to be similar, while the brightness of the HF-device is slightly lower (Figure 5b). The performance is comparable in the two cases and the EQE is divided into two regimes; below 1 mA cm^{-2} where the EQE is higher in the HF-OLED ($\approx 30\%$); and above 1 mA cm^{-2} where the EQE is higher in the TADF only OLED (Figure 5c). Further, v-DABNA OLEDs in mCBPCN host were fabricated using the same device structure and although they cannot compete with the previously reported devices using DOBNA-OAr as a host,^[43] they also show the common MR-TADF EQE response, with two different regimes (Figure S26, Supporting Information); a high performance one below 1 mA cm^{-2} and one above with low performance. The latter implies that at higher current densities the longer-lived DF lifetime of the v-DABNA terminal emitter results in excess triplet quenching mechanisms.

Focusing on the EL spectra one can observe that although there is a clear contribution of the sensitizer $\approx 500 \text{ nm}$

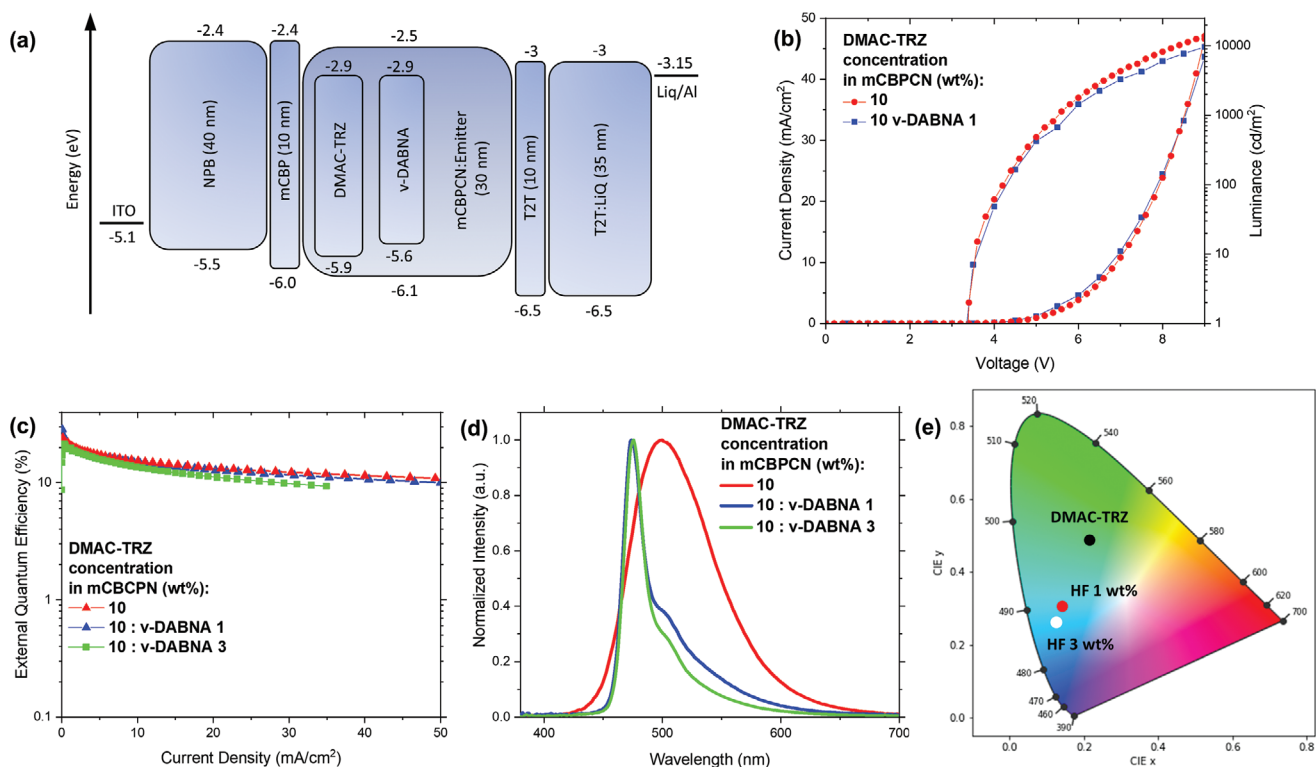


Figure 5. OLEDs performance. a) Device architecture, b) JVL curves, and c) EQE versus current density of TADF only and HF OLEDs. d) EL spectra and e) CIE coordinates collected at 8 V.

(Figure 5d), the results are comparable or even better compared to previously published studies using deeper blue sensitizers with similar quantum yield.^[44,45] This does not seem possible considering the relatively lower FRET efficiency of the specific set of DMAC-TRZ/v-DABNA system. Thus, we suggest that the presence of the QA conformer acts as an extra (sensitizer emission) component that directly pumps the terminal emitter through efficient FRET, instead of just the QE conformer as seen in TADF only devices. The QA conformer PL spectrum has much better overlap with the v-DABNA absorption spectrum, compared to the QE absorption spectrum (Figure S25b,c, Supporting Information). Further, another important parameter for a high FRET radius is the extinction coefficient of the acceptor, which is orders of magnitude higher in v-DABNA. The FRET radius^[32] from the QA conformer to the QE conformer or the terminal emitter (v-DABNA) was calculated to be 2.3 and 4.05 nm respectively. As a result, the energy of the initial QA population is expected to be mainly transferred to the v-DABNA molecules and not the QE configuration. FRET from the QE conformer to the terminal emitter is still occurring (Figure S25a, Supporting Information), but the efficiency is lower compared to the QA to terminal emitter energy transfer. To investigate further the energy transfer efficiency of the QE conformer to the terminal emitter, especially in the DF regime where triplet harvesting is critical for the OLED performance, time-resolved measurements in three different systems are shown in Figure S27a (Supporting Information). The HF-system (DMAC-TRZ:v-DABNA in mCBPCN) shows a small quenching of the late PF and early DF lifetime, compared to the DMAC-TRZ film but a much stronger quenching of longer DF contribution, following the v-DABNA film lifetime. The latter indicates that we have two different regimes, one with high and one with low FRET efficiency from the QE conformer to the terminal emitter. From the contour plot of the HF-system (Figure S27b, Supporting Information), one can observe a second spectral band increasing in the less efficient energy transfer regime ($15 < t < 1000$ ns). In the PF regime, the early time spectrum has an identical shape with the v-DABNA film, confirming the high FRET efficiency of the QA conformer to the terminal emitter (Figure S27c, Supporting Information). At later times, the second band appears and contributes equally to the PL spectrum as the terminal emitter. This is the effect of the more orthogonal D-A QE conformers, that have longer wavelength emission and longer PF lifetime as shown before.^[23] In the DF regime, the opposite occurs. The longer wavelength QE conformer have shorter lifetime and can be seen at early DF times, thus can be observed in the HF system (Figure S27d, Supporting Information). Over time, only the shorter wavelength QE conformers decay radiatively and have better spectral overlap with the terminal emitter, thus the PL emission mainly originates from v-DABNA. This implies that the FRET efficiency between the QE conformer and the terminal emitter is highly inhomogeneous and is entirely dependent on the dihedral angle distribution of the QE conformers. At late PF and early DF regimes the FRET efficiency will be relatively poor, while at early PF and late DF the efficiency will be higher, with a FRET radius of 3.45 nm. This less efficient energy transfer process results in a very small contribution of

the QE emission in the overall EL spectrum, at 1 wt.% concentration of v-DABNA (Figure 5d).

With increasing terminal emitter concentration, an increase of FRET efficiency occurs resulting in a smaller contribution of the TADF sensitizer as observed in the EL spectrum (Figure 5d) and is much closer to the v-DABNA only OLED (Figure S26a, Supporting Information). The EL spectra of both HF OLEDs (1 and 3 wt.% concentration) are stable with increasing voltage/current density (Figure S28, Supporting Information), excluding the presence of a current density dependent band and/or the contribution from and interfacial exciplex EL emission. The maximum EQE decreases with increased concentration, which we assume is, among other effects, due to stronger intermolecular interactions and excimer quenching,^[32] but is still above 20%. The color coordinates shifted from (0.21, 0.47) to (0.16, 0.31) and (0.14, 0.27) in DMAC-TRZ only, HF OLED 1 and 3 wt.% respectively (Figure 5e). To our understanding this is the first set of HF OLEDs that convert green EL emission to blue.

3. Conclusion

DMAC-TRZ has been studied extensively before, but there are many aspects of its photophysics and device performance that have not been revealed until now.^[18,22,23,31,35,46,47] The presence of a second conformer, the QA, has proven to be stronger than expected and its contribution to the photophysical performance in solid-state, especially at low concentrations, has proven to be dominant. At higher concentrations (above 1 wt.%), the FRET efficiency to the QE conformer increases greatly and its contribution cannot be easily observed, this could be why it was not observed until now. A key parameter for its strong contribution is the presence of a rigid host, that hinders possible conformational relaxation to the QE conformation, with the presence of excess (excitation) energy. The sensitivity of the two conformers to the environment appears to be different, indicating a stronger local character for the QA and a stronger CT character for the QE conformer, verified by quantum chemical calculations. The DF appears to originate purely from the QE conformer mainly because of the high ΔE_{ST} of the QA preventing the formation of rISC channels from the T_1 to S_1 . Intermolecular interactions (dimer/excimer formation) improve the rISC rate and show that can be more efficient compared to the monomer performance. The triplet value mystery of DMAC-TRZ (the triplet is lower in energy than either the D or A units) has been resolved, with experimental proofs showing that the actual triplet value observed in DMAC-TRZ systems originates from the QA conformer and not the QE. OLEDs of DMAC-TRZ show the contribution of the QA conformer to the EL spectrum of the device, only in specific environments and low concentrations. To explore the energy transfer process of the two conformers, HF-devices using v-DABNA as the terminal emitter show high relative FRET efficiency compared to similar systems,^[44,45] indicating that the QA conformer transfers its energy directly to the terminal emitter instead of the QE conformer. The efficient energy transfer resulted to the fabrication of the first OLEDs that convert green EL emission into blue using the HF approach.

Supporting Information

Supporting Information is available from the Wiley Online Library or from the author.

Acknowledgements

The authors thank Prof. Takuji Hatakeyama for providing the v-DABNA emitter. This project had received funding from the European Union's Horizon 2020 research and innovation programme under the Marie Skłodowska Curie grant agreement No 812872 (TADFlife). T.B., L.M.D., and C.M.M. acknowledge the Deutsche Forschungsgemeinschaft (DFG, German Research Foundation) – 396890929/GRK 2482 and MA1051/17-1. A.P.M. thanks the EPSRC for funding, EP/T02240X/1.

Conflict of Interest

The authors declare no conflict of interest.

Data Availability Statement

The data that support the findings of this study are available in the supplementary material of this article.

Keywords

acridine, dual conformations, FRET, hyperfluorescence, OLED, quasi-axial, TADFs

Received: January 25, 2023

Revised: February 16, 2023

Published online:

- [1] Z. Yang, Z. Mao, Z. Xie, Y. Zhang, S. Liu, J. Zhao, J. Xu, Z. Chi, M. P. Aldred, *Chem. Soc. Rev.* **2017**, *46*, 915.
- [2] C. Adachi, M. A. Baldo, M. E. Thompson, S. R. Forrest, *J. Appl. Phys.* **2001**, *90*, 5048.
- [3] J. R. Lakowicz, *Principles of Fluorescence Spectroscopy*, 3rd ed., Springer, New York **2006**.
- [4] G. Méhes, H. Nomura, Q. Zhang, T. Nakagawa, C. Adachi, *Angew. Chem., Int. Ed.* **2012**, *51*, 11311.
- [5] H. Wang, L. Xie, Q. Peng, L. Meng, Y. Wang, Y. Yi, P. Wang, *Adv. Mater.* **2014**, *26*, 5198.
- [6] Y. Liu, G. Zhan, Z. W. Liu, Z. Q. Bian, C. H. Huang, *Chin. Chem. Lett.* **2016**, *27*, 1231.
- [7] F. B. Dias, K. N. Bourdakos, V. Jankus, K. C. Moss, K. T. Kamtekar, V. Bhalla, J. Santos, M. R. Bryce, A. P. Monkman, *Adv. Mater.* **2013**, *25*, 3707.
- [8] M. A. Baldo, D. F. O'Brien, Y. You, A. Shoustikov, S. Sibley, M. E. Thompson, S. R. Forrest, *Nature* **1998**, *395*, 151.
- [9] P. L. Santos, J. S. Ward, P. Data, A. S. Batsanov, M. R. Bryce, F. B. Dias, A. P. Monkman, *J. Mater. Chem. C* **2016**, *4*, 3815.
- [10] F. B. Dias, T. J. Penfold, A. P. Monkman, *Methods Appl. Fluoresc.* **2017**, *5*, 012001.
- [11] M. K. Etherington, J. Gibson, H. F. Higginbotham, T. J. Penfold, A. P. Monkman, *Nat. Commun.* **2016**, *7*, 13680.
- [12] T. J. Penfold, E. Gindensperger, C. Daniel, C. M. Marian, *Chem. Rev.* **2018**, *118*, 6975.
- [13] Z. R. Grabowski, K. Rotkiewicz, W. Rettig, *Chem. Rev.* **2003**, *103*, 3899.
- [14] L.-S. Cui, H. Nomura, Y. Geng, J. U. Kim, H. Nakanotani, C. Adachi, *Angew. Chem., Int. Ed.* **2017**, *56*, 1571.
- [15] Y. Tao, K. Yuan, T. Chen, P. Xu, H. Li, R. Chen, C. Zheng, L. Zhang, W. Huang, *Adv. Mater.* **2014**, *26*, 7931.
- [16] F. B. Dias, J. Santos, D. R. Graves, P. Data, R. S. Nobuyasu, M. A. Fox, A. S. Batsanov, T. Palmeira, M. N. Berberan-Santos, M. R. Bryce, A. P. Monkman, *Adv. Sci.* **2016**, *3*, 1600080.
- [17] X. Cai, B. Gao, X. L. Li, Y. Cao, S. J. Su, *Adv. Funct. Mater.* **2016**, *26*, 8042.
- [18] T.-A. Lin, T. Chatterjee, W.-L. Tsai, W.-K. Lee, M.-J. Wu, M. Jiao, K.-C. Pan, C.-L. Yi, C.-L. Chung, K.-T. Wong, C.-C. Wu, *Adv. Mater.* **2016**, *28*, 6976.
- [19] P. L. dos Santos, J. S. Ward, D. G. Congrave, A. S. Batsanov, J. Eng, J. E. Stacey, T. J. Penfold, A. P. Monkman, M. R. Bryce, *Adv. Sci.* **2018**, *5*, 1700989.
- [20] L. Yu, Z. Wu, G. Xie, C. Zhong, Z. Zhu, H. Cong, D. Ma, C. Yang, *Chem. Commun.* **2016**, *52*, 11012.
- [21] V. Jankus, P. Data, D. Graves, C. McGuinness, J. Santos, M. R. Bryce, F. B. Dias, A. P. Monkman, *Adv. Funct. Mater.* **2014**, *24*, 6178.
- [22] D. K. A. Phan Huu, S. Saseendran, R. Dhali, L. G. Franca, K. Stavrou, A. Monkman, A. Painelli, *J. Am. Chem. Soc.* **2022**, *144*, 15211.
- [23] K. Stavrou, L. G. Franca, A. P. Monkman, *ACS Appl. Electron. Mater.* **2020**, *2*, 2868.
- [24] D. Kelly, L. G. Franca, K. Stavrou, A. Danos, A. P. Monkman, *J. Phys. Chem. Lett.* **2022**, *13*, 6981.
- [25] H. Tanaka, K. Shizu, H. Nakanotani, C. Adachi, *J. Phys. Chem. C* **2014**, *118*, 15985.
- [26] M. K. Etherington, F. Franchello, J. Gibson, T. Northey, J. Santos, J. S. Ward, H. F. Higginbotham, P. Data, A. Kurowska, P. L. Dos Santos, D. R. Graves, A. S. Batsanov, F. B. Dias, M. R. Bryce, T. J. Penfold, A. P. Monkman, *Nat. Commun.* **2017**, *8*, 14987.
- [27] Y. Z. Shi, K. Wang, S. L. Zhang, X. C. Fan, Y. Tsuchiya, Y. T. Lee, G. L. e Dai, J. X. Chen, C. J. Zheng, S. Y. Xiong, X. M. Ou, J. Yu, J. S. Jie, C. S. Lee, C. Adachi, X. H. Zhang, *Angew. Chem., Int. Ed.* **2021**, *60*, 25878.
- [28] W. Li, X. Cai, B. Li, L. Gan, Y. He, K. Liu, D. Chen, Y. C. Wu, S. J. Su, *Angew. Chem., Int. Ed.* **2019**, *58*, 582.
- [29] K. Wang, C.-J. Zheng, W. Liu, K. Liang, Y.-Z. Shi, S.-L. Tao, C.-S. Lee, X.-M. Ou, X.-H. Zhang, *Adv. Mater.* **2017**, *29*, 1701476.
- [30] I. Marghad, F. Bencheikh, C. Wang, S. Manolikakes, A. Rérat, C. Gosmini, D. H. Kim, J. C. Ribierre, C. Adachi, *RSC Adv.* **2019**, *9*, 4336.
- [31] W. L. Tsai, M. H. Huang, W. K. Lee, Y. J. Hsu, K. C. Pan, Y. H. Huang, H. C. Ting, M. Sarma, Y. Y. Ho, H. C. Hu, C. C. Chen, M. T. Lee, K. T. Wong, C. C. Wu, *Chem. Commun.* **2015**, *51*, 13662.
- [32] K. Stavrou, A. Danos, T. Hama, T. Hatakeyama, A. Monkman, *ACS Appl. Mater. Interfaces* **2021**, *13*, 8643.
- [33] K. Stavrou, S. Madayanad Suresh, D. Hall, A. Danos, N. A. Kukhta, A. M. Z. Slawin, S. Warriner, D. Beljonne, Y. Olivier, A. Monkman, E. Zysman-Colman, *Adv. Opt. Mater.* **2022**, *10*, 2200688.
- [34] D. Hall, K. Stavrou, E. Duda, A. Danos, S. Bagnich, S. Warriner, A. M. Z. Slawin, D. Beljonne, A. Köhler, A. Monkman, Y. Olivier, E. Zysman-Colman, *Mater. Horiz.* **2022**, *9*, 1068.
- [35] R. Dhali, D. K. A. Phan Huu, F. Bertocchi, C. Sissa, F. Terenziani, A. Painelli, *Phys. Chem. Chem. Phys.* **2021**, *23*, 378.
- [36] Y. Qian, X. Li, A. R. Harutyunyan, G. Chen, Y. Rao, H. Chen, *J. Phys. Chem. A* **2020**, *124*, 9156.
- [37] J. Gibson, A. P. Monkman, T. J. Penfold, *ChemPhysChem* **2016**, *17*, 2956.
- [38] D. De Sa Pereira, C. Menelaou, A. Danos, C. Marian, A. P. Monkman, *J. Phys. Chem. Lett.* **2019**, *10*, 3205.

- [39] Y. Wada, H. Nakagawa, S. Matsumoto, Y. Wakisaka, H. Kaji, *Nat. Photonics* **2020**, *14*, 643.
- [40] J. M. Kaminski, A. Rodríguez-Serrano, F. Dinkelbach, H. Miranda-Salinas, A. P. Monkman, C. M. Marian, *Chem. Sci.* **2022**, *13*, 7057.
- [41] J. Zhang, D. Ding, Y. Wei, H. Xu, *Chem. Sci.* **2016**, *7*, 2870.
- [42] T. Förster, *Ann. Phys.* **1948**, *437*, 55.
- [43] Y. Kondo, K. Yoshiura, S. Kitera, H. Nishi, S. Oda, H. Gotoh, Y. Sasada, M. Yanai, T. Hatakeyama, *Nat. Photonics* **2019**, *13*, 678.
- [44] S. O. Jeon, K. H. Lee, J. S. Kim, S. G. Ihn, Y. S. Chung, J. W. Kim, H. Lee, S. Kim, H. Choi, J. Y. Lee, *Nat. Photonics* **2021**, *15*, 208.
- [45] C. Y. Chan, M. Tanaka, Y. T. Lee, Y. W. Wong, H. Nakanotani, T. Hatakeyama, C. Adachi, *Nat. Photonics* **2021**, *15*, 203.
- [46] Y. Wada, K. Shizu, S. Kubo, T. Fukushima, T. Miwa, H. Tanaka, C. Adachi, H. Kaji, **2016**, *9*, 032102.
- [47] Y. Wada, H. Nakagawa, H. Kaji, *Chem. – Asian J.* **2021**, *16*, 1073.